High-Aspect-Ratio Laser-Fusion Targets Driven by 24-Beam uv Laser Radiation

M. C. Richardson, P. W. McKenty, R. L. Keck, F. J. Marshall, D. M. Roback, C. P. Verdon, R. L. McCrory, and J. M. Soures

Laboratory for Laser Energetics, University of Rochester, Rochester, New York 14623

and

S. M. Lane

Lawrence Livermore National Laboratory, University of California, Livermore, Livermore, California 94550

(Received 3 March 1986)

The implosions of thin-walled, large-diameter, deuterium-tritium–filled glass microballoon targets ablatively driven by the 351-nm, 2-kJ OMEGA laser are reported. Compressed-fuel diagnostics, including the first direct simultaneous measurements of the fuel and shell areal densities, and detailed hydrodynamic simulations determine the effect of illumination uniformity on implosion symmetry.

PACS numbers: 52.50.Jm

Direct-drive laser fusion requires the uniform compression of spherical DT fuel pellets to densities >2000 times liquid density by the creation of a high-temperature, ablating, thermalized plasma uniformly around the imploding target. Many experimental and theoretical studies have established the advantages of short-wavelength laser radiation for effective coupling of the laser energy into a high-density collisional plasma,[1-5] without the generation of copious superthermal electrons,[5,6] and the creation of high ablation pressures[7] >50 Mbar for efficient compressions on low isentropes. However, simple heuristic arguments[8] and predictions of two-dimensional hydrodynamic simulations show that the implosion symmetry of spherical shell targets driven to high final core densities will only be maintained for modest initial ratios $(R/\Delta R)_0$ of shell radius (R) to thickness (ΔR) under a high degree $(\sigma_{\rm rms} < 1\%)$ of illumination uniformity.

The implosions of large-$(R/\Delta R)_0$ targets driven by nanosecond 351-nm radiation at low intensities $(<2\times10^{14}$ W/cm$^2)$ are of interest for several reasons. At these intensities the primary coupling mechanism is inverse-bremsstrahlung absorption, and parametric processes producing hot electrons capable of preheating the fuel are below threshold.[9] Optimal performance of these targets results in the acceleration of low-mass shells to high velocities, leading to high compressed-core temperatures and high neutron yields. The latter permits the deployment of diagnostics of the fuel and shell areal densities.

In this paper we describe the first set of direct-drive ablative-target implosion experiments produced by the symmetric multibeam (24), 2.5-kJ, uv (351 nm) OMEGA laser system. These experiments used large-diameter, large-aspect-ratio $[(R/\Delta R)_0 \sim 200]$ DT-filled glass microballoons. A large number of plasma, x-ray, and nuclear diagnostics were used in these experiments; however, in this communication, emphasis is placed on those which diagnose the final core conditions. Neutron yields in these experiments were as high as 2.06×10^{11}. Simulations of these experiments were made with the one-dimensional hydrodynamic code LILAC,[10] and the two-dimensional hydrodynamic code, ORCHID, both of which include tabular equation-of-state (SESAME),[11] flux-limited electron thermal transport,[12] multifrequency group radiation transport with local thermodynamic equilibrium opacities,[13] and inverse-bremsstrahlung–absorption energy deposition through a ray-tracing algorithm[14] in the underdense plasma.

The predicted behavior of a typical target of ~750 μm diameter and $(R/\Delta R)_0 = 185$, filled with DT (10 atm) and irradiated with 2.2 kJ of 351-nm radiation in a 600-ps (FWHM) Gaussian pulse is shown in Fig. 1. Although $(R/\Delta R)_0$ is initially high, rapid expansion of the shell [Fig. 1(a)] occurs during the acceleration phase, resulting in a modest in-flight aspect ratio[15] (~20) at the midradius point [Fig. 1(b)]. Absorption of the laser radiation occurs efficiently $(\sim80\%)$, principally during the first half of the implosion [Fig. 1(c)], with intensities at the critical-density surface $(n_e \sim 10^{22}$ cm$^{-3})$ never exceeding 1.0×10^{14} W/cm^2 [Fig. 1(d)]. Neutron generation commences with the convergence of the first shock and results in a maximum yield of 2.4×10^{12} [Fig. 1(e)]. Upon stagnation, the average DT-ion temperature is ~6 keV with a modest peak density of ~0.7 g/cm^3 [Fig. 1(f)]. The rapid rises of the shell and fuel areal densities are shown in Figs. 1(g) and 1(h).

The implosion experiments were made on DT-filled (10 atm), 700–800-μm-diam, glass microballoon targets having a wall thickness in the range of 1.3–2.1 μm. Up to 2.5 kJ in 700-ps pulses (FWHM) with 3% beam-energy variance from the OMEGA system[16,17] was focused on target with 566-mm focal length $(f/3.7)$ single-lens optics having lateral and axial posi-

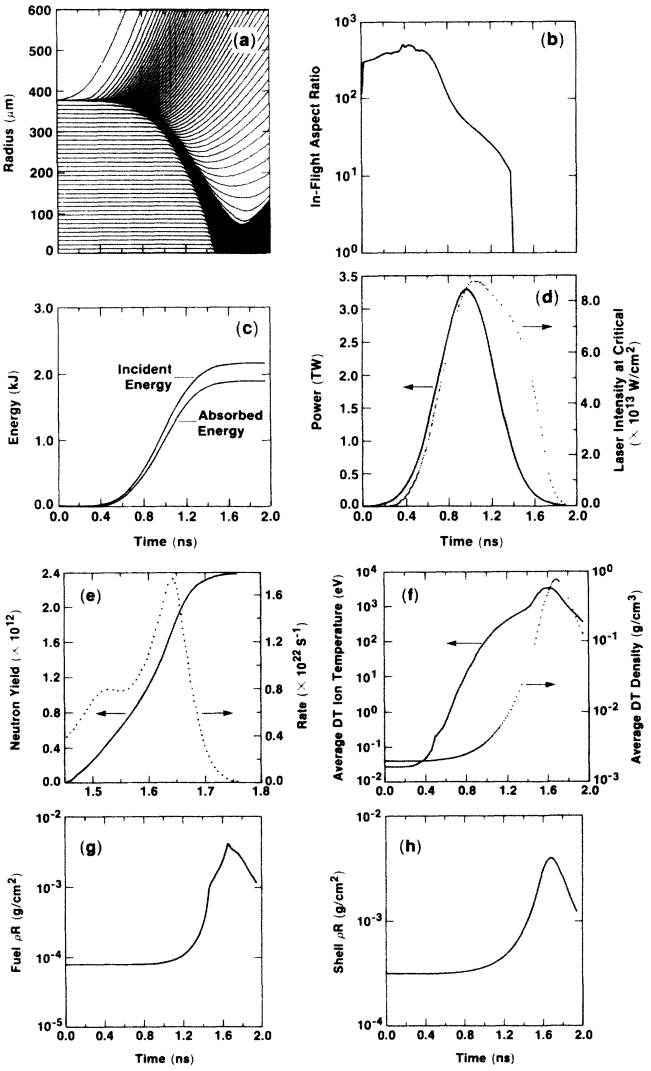

FIG. 1. One-dimensional LILAC simulations of the implosion of a DT-filled (10 atm), 700-μm-diameter, 2-μm-wall glass microballoon irradiated with 2-kJ, 700-ps pulses of 351-nm laser light. (a) The R-T plot of the Lagrangean elements. (b) The in-flight-aspect ratio. (c) The integrated fractional absorption. (d) The intensity at the critical surface as a function of time during the implosion. (e) The integrated and rate of generation of neutrons. (f) The average ion temperature and density. (g) The average fuel areal density. (h) The average shell areal density.

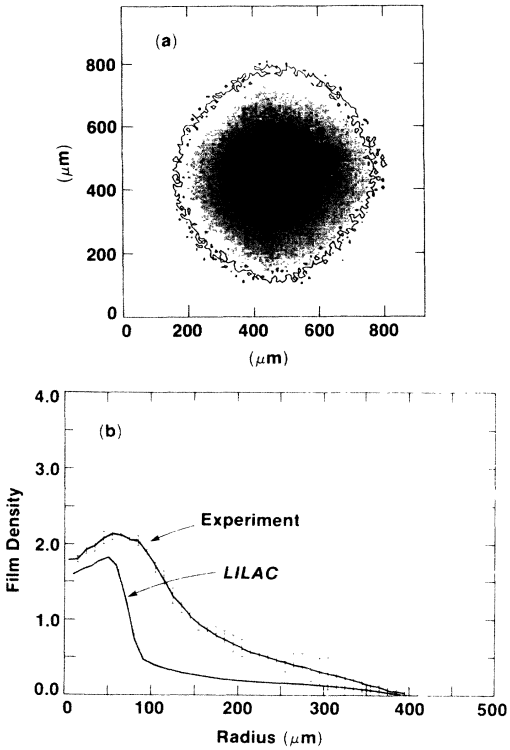

FIG. 2. Comparison of measured and predicted x-ray image distributions. (a) A contoured and shaded representation of an x-ray micrograph of a target implosion. The initial target diameter was 760 μm; the micrograph shows x-ray emission predominantly from a stagnated core ~ 125 μm in diameter. (b) The equivalent one-dimensional measurements, as determined by the azimuthal average of the film-density distribution about the implosion center, compared to the LILAC prediction.

tional accuracies of 20 and 50 μm, respectively. From a characterization of the beam intensity distribution in the target plane,[18] the illumination nonuniformity ($\sigma_{\rm rms}$) was estimated to be $\sim 15\%$ (rms) for all beams focused 10 target radii ($F=10R$) beyond the target center, with corresponding peak-to-valley intensity variations of $\sim 60\%$. The overall absorption, measured with an array of twenty differential plasma calorimeters, was $\sim 80\%$. Measurements of the continuum x-ray emission spectrum indicated, as with earlier six-beam experiments on solid spherical targets,[5] that less than 10^{-4} of the absorbed energy was coupled to collisionless superthermal electrons.

Final compressed-target conditions were inferred from a number of x-ray and neutron diagnostics described fully elsewhere.[19] Figure 2(a) shows film-density contours superimposed on a digitized (~ 4 keV) x-ray micrograph. Much of the x-ray emission originates from a central ring, ~ 125 μm in diameter, from the target shell during the final stages of the implosion. Figure 2(b) shows a comparison of the azimuthal average of the film density versus radius from the image of the implosion of shot No. 11233, and the radial profile predicted by LILAC. This target was irradiated with $F=6R$, for which an overall $\sigma_{\rm rms} \sim 20\%$ is estimated. The larger diameter of the measured x-ray emission from the stagnated core is probably due to departures from spherical symmetry as described below. Neutron activation of compressed shell material via the reaction[20] ^{28}Si$(n,p)^{28}$Al provided a measure of the shell $\langle \rho \Delta R \rangle$; spectrometry of DT ions scattered by 14.1-MeV neutrons[21] was used to estimate $\langle \rho R \rangle$.[19]

TABLE I. Neutron yield and fuel and shell areal densities.

Shot No.	$10^{10} Y_n$		$\langle \rho R \rangle$ (10^{-4} g/cm^2)		$\langle \rho \Delta R \rangle$ (10^{-4} g/cm^2)	
	Expt.	LILAC	Expt.	LILAC	Expt.	LILAC
11200	2.70	124	5.8 ± 10	25.0	11.0 ± 1.0	31.6
11233	11.30	233	21.3 ± 4.4	25.1	· · ·	27.5
11306	20.60	801	· · ·	39.5	· · ·	33.8
11309	1.93	92	71.4 ± 14.0	25.7	10.0 ± 1.0	38.3
11310	6.70	244	· · ·	31.4	20.7 ± 0.8	38.0
11311	13.20	416	· · ·	34.1	15.3 ± 0.6	36.6

This technique is most suitable for targets such as those used here, where negligible moderation of the DT-ion energy distribution occurs in the fuel and compressed shell.[22] A technique using neutron activation of ^{80}Kr tracer gas in the fuel[23] is under development for targets which do not satisfy this condition.[24]

An understanding of the effects of implosion nonuniformities on the final core conditions is obtained by comparing experimental data with LILAC and ORCHID code simulations. Table I shows that the measured shell $\langle \rho \Delta R \rangle$ values are consistently less than those predicted for perfect symmetry, while there is more variability in the measured fuel $\langle \rho R \rangle$. The greatest disparity occurs in the neutron yield. Moreover, the average ion temperature (T_i), deduced from neutron time-of-flight spectrometry,[19] $T_i \sim 3.5$ keV, was significantly less than predicted, Fig. 1(f). Much closer agreement with experiments is obtained with the two-dimensional code ORCHID, when account is taken of the estimated illumination uniformity. This was approximated by the assumption of contributions from the three dominant spherical harmonic (l) modes, $l = 2$, 4, and 8, totaling an overall $\sigma_{\rm rms} \sim 12.5\%$. An ORCHID simulation of shot No. 11233, Fig. 3, shows that serious deformation (48% peak to valley) of the shell has occurred by the time the shell stagnates, Fig 3(b). However, despite this level of implosion asymmetry, Fig. 3(c), the entire fuel region has a density of ~ 0.5 g/cm^3, and an overall fuel $\langle \rho R \rangle \sim 1.5 \times 10^{-3}$ g/cm^2, comparable to those in Table I. Moreover, the predicted values for the neutron yield and average ion temperature, 5×10^{11} and 4.2 keV, respectively, are close to those measured. An explanation for the reduced thermonuclear burn conditions is gained from the velocity vector diagram superimposed on the Lagrangean mesh, at stagnation, Fig. 3(d). This shows considerable material swirling, indicating the likelihood of high-Z shell material being transported into the fuel, lowering the fuel-ion temperature, and partially quenching the thermonuclear burn.

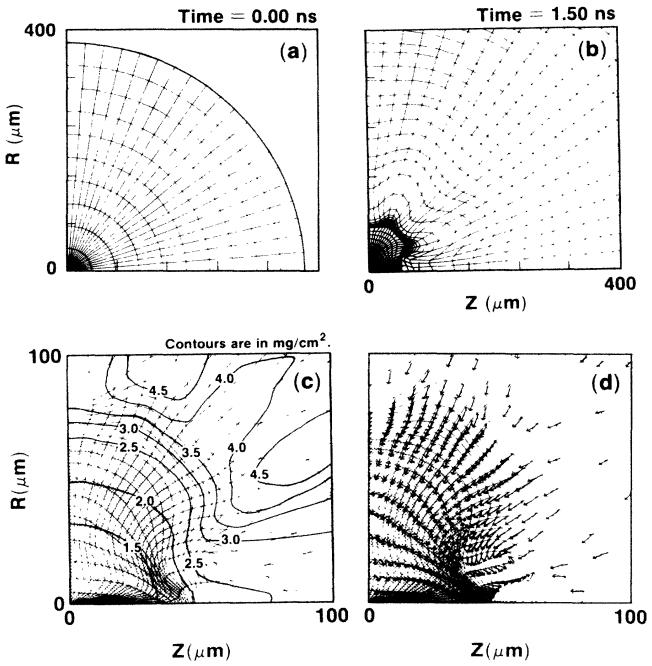

FIG. 3. Two-dimensional hydrodynamic code, ORCHID, simulations of shot No. 11233. (a),(b) The mesh plot at $t = 0$ and $t = 1.50$ ns. (c) An expanded view of (b) with contours of constant areal density superimposed. (d) The fluid-velocity vector plot at 1.50 ns, superimposed on the mesh plot, where the fuel region has been shaded.

These experiments establish for ablatively driven high-aspect-ratio targets a quantifiable relationship between illumination uniformity implosion symmetry and final core conditions. They show that the peak final density can only be estimated with confidence through simultaneous measurement of core conditions, particularly the fuel and shell areal densities. By comparison of these measurements with numerical simulations a perspective on the complex processes occurring in the compressed target can be obtained.

The authors acknowledge the support of the Laser Operations, Experimental, and Target Fabrication groups of the Laboratory for Laser Energetics. All targets used in this study were fabricated and DT-filled by KMS Fusion, Inc. This work was supported by the U.S. Department of Energy Office of Inertial Fusion under Agreement No. DE-FC08-85DP40200 and by

the Laser Fusion Feasibility Project at the Laboratory for Laser Energetics, which has the following sponsors: Empire State Electric Energy Research Corporation, General Electric Company, New York State Energy Research and Development Authority, Ontario Hydro, Southern California Edison Company, and the University of Rochester.

[1]D. C. Slater *et al.*, Phys. Rev. Lett. **46**, 1199 (1981).
[2]W. C. Mead *et al.*, Phys. Rev. Lett. **47**, 1289 (1981).
[3]W. Seka *et al.*, Opt. Commun. **40**, 437 (1982).
[4]C. Garban-Labaune *et al.*, Phys. Rev. Lett. **48**, 1018 (1982).
[5]M. C. Richardson *et al.*, Phys. Rev. Lett. **54**, 1656 (1985).
[6]R. L. Keck *et al.*, Phys. Fluids **27**, 2762 (1984).
[7]B. Yaakobi *et al.*, J. Appl. Phys. **57**, 4354 (1985).
[8]J. Nuckols *et al.*, Nature (London) **239**, 139 (1972).
[9]A. Simon *et al.*, Phys. Fluids **26**, 3107 (1983).
[10]Laboratory for Laser Energetics, University of Rochester, Report No. 16, 1976 (unpublished).
[11]B. I. Bennett, J. D. Johnson, G. T. Kirley, and G. T. Rand, Los Alamos National Laboratory Report No. LA-7130, 1978 (unpublished).
[12]R. C. Malone, R. L. McCrory, and R. L. Morse, Phys. Rev. Lett. **34**, 721 (1975).
[13]W. F. Henbner, A. L. Mertz, N. A. Magec, Jr., and M. F. Argo, Los Alamos National Laboratory Report No. LA-6760-M, 1977 (unpublished).
[14]M. Born and E. Wolf, *Principles of Optics* (Pergamon, New York, 1975), p. 123.
[15]The in-flight aspect ratio is here defined as the mean radius of 80% of the shell mass divided by its thickness.
[16]J. M. Soures, R. J. Hutchison, S. D. Jacobs, L. D. Lund, R. L. McCrory, and M. C. Richardson, in *Proceedings of the Tenth Symposium on Fusion Energy, Philadelphia, 5–9 December 1983* (IEEE, New York, 1983), p. 1392.
[17]M. C. Richardson *et al.*, in *1985 Conference on Lasers and Electro-Optics (CLEO-85) Technical Digest* (Optical Society of America, Washington, D.C., 1985), p. 234.
[18]Laboratory for Laser Energetics, University of Rochester, Quarterly Report No. 23, 1985 (unpublished), p. 103.
[19]M. C. Richardson *et al.*, in "Laser Interaction and Related Plasma Phenomena," edited by H. Hora and G. H. Miley (Plenum, New York, to be published), Vol. 7.
[20]S. M. Lane *et al.*, Appl. Phys. Lett. **37**, 600 (1980).
[21]S. Kacenjar *et al.*, Phys. Rev. Lett. **49**, 463 (1982).
[22]S. Kacenjar *et al.*, J. Appl. Phys. **56**, 2027 (1984).
[23]E. M. Campbell *et al.*, J. Appl. Phys. **51**, 6062 (1980).
[24]S. Prussin, S. M. Lane, C. Bennett, M. C. Richardson, and S. Noyes, post deadline presentation at the Annual Meeting of the Division of Plasma Physics of the American Physical Society, San Diego, 1985 (unpublished).

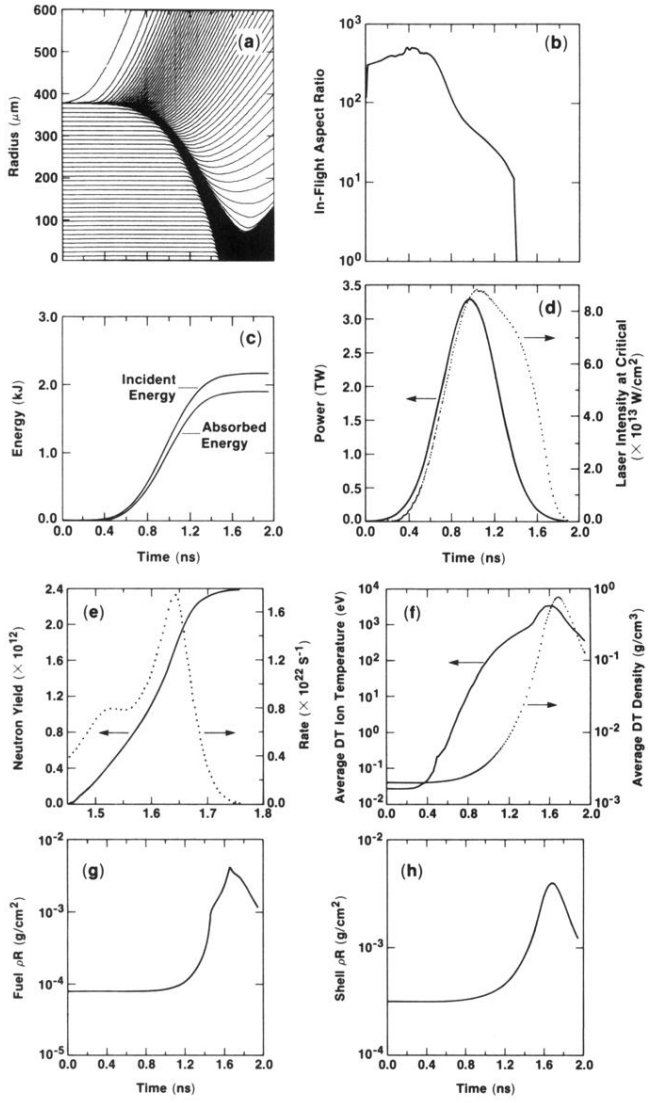

FIG. 1. One-dimensional LILAC simulations of the implosion of a DT-filled (10 atm), 700-μm-diameter, 2-μm-wall glass microballoon irradiated with 2-kJ, 700-ps pulses of 351-nm laser light. (a) The R-T plot of the Lagrangean elements. (b) The in-flight-aspect ratio. (c) The integrated fractional absorption. (d) The intensity at the critical surface as a function of time during the implosion. (e) The integrated and rate of generation of neutrons. (f) The average ion temperature and density. (g) The average fuel areal density. (h) The average shell areal density.

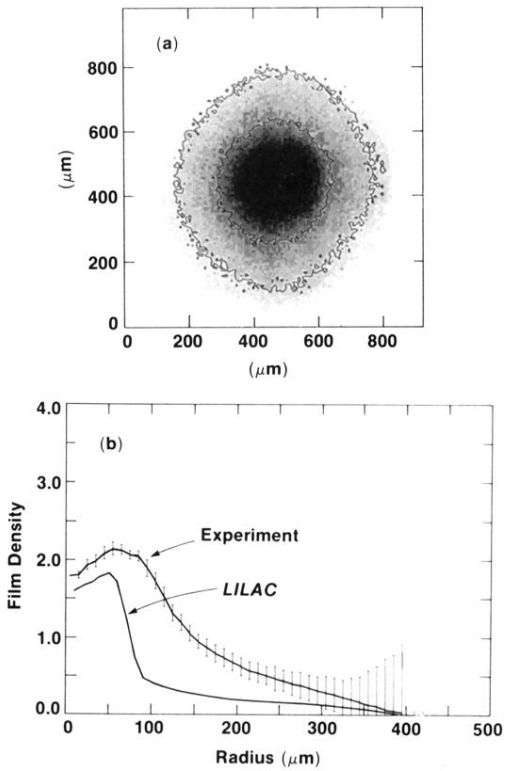

FIG. 2. Comparison of measured and predicted x-ray image distributions. (a) A contoured and shaded representation of an x-ray micrograph of a target implosion. The initial target diameter was 760 μm; the micrograph shows x-ray emission predominantly from a stagnated core ~ 125 μm in diameter. (b) The equivalent one-dimensional measurements, as determined by the azimuthal average of the film-density distribution about the implosion center, compared to the LILAC prediction.

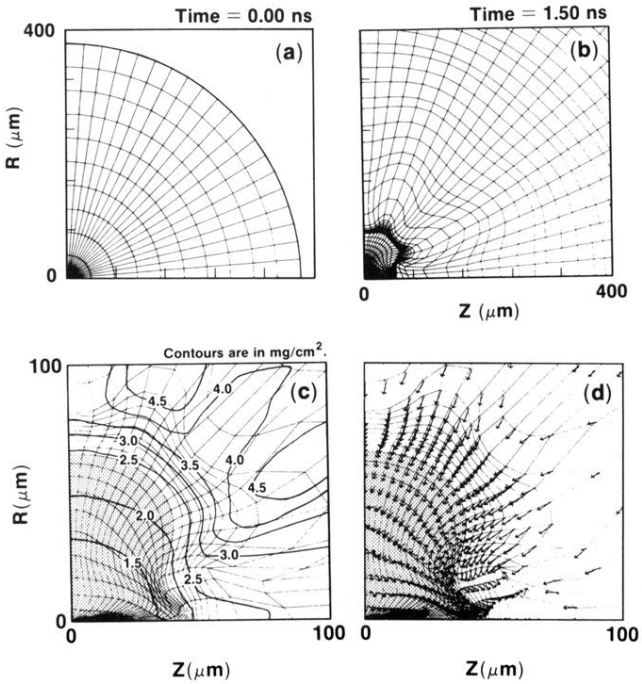

FIG. 3. Two-dimensional hydrodynamic code, ORCHID, simulations of shot No. 11233. (a),(b) The mesh plot at $t = 0$ and $t = 1.50$ ns. (c) An expanded view of (b) with contours of constant areal density superimposed. (d) The fluid-velocity vector plot at 1.50 ns, superimposed on the mesh plot, where the fuel region has been shaded.